AGU PUBLICATIONS

Geophysical Research Letters

RESEARCH LETTER
10.1002/2015GL065974

Key Points:
- The low-frequency variability at decadal timescales is robust in the presence of a seasonal cycle
- The summer ocean mixed layer depth plays a key role in the emergence of the LFV
- The mean depth of the ocean mixed layer controls the period of the low-frequency variability

Supporting Information:
- Supporting Information S1

Correspondence to:
S. Vannitsem,
svn@meteo.be

Citation:
Vannitsem, S. (2015), The role of the ocean mixed layer on the development of the North Atlantic Oscillation: A dynamical system's perspective, *Geophys. Res. Lett.*, *42*, 8615–8623, doi:10.1002/2015GL065974.

Received 28 AUG 2015
Accepted 2 OCT 2015
Accepted article online 5 OCT 2015
Published online 24 OCT 2015

The role of the ocean mixed layer on the development of the North Atlantic Oscillation: A dynamical system's perspective

Stéphane Vannitsem[1]

[1]Institut Royal Météorologique de Belgique, Brussels, Belgium

Abstract The development of the low-frequency variability (LFV) in the atmosphere at multidecadal timescales is investigated in the context of a low-order coupled ocean-atmosphere model designed to emulate the interaction between the ocean mixed layer (OML) and the atmosphere at midlatitudes, both subject to seasonal variations of the Sun's radiative input. When no seasonal dependences are present, a LFV is emerging from the chaotic background for sufficiently large wind stress forcing (WSF). The period of this LFV is strongly controlled by the depth of the OML, with a shorter period for a deeper layer. In the seasonally dependent case, a similar LFV is developing that persists throughout the year. Remarkably, the emergence of this LFV occurs for smaller values of the WSF coefficient and is strongly related to the small thickness of the OML in summer, i.e., large impact of the WSF. Potential implications for real-world dynamics are discussed.

1. Introduction

The atmosphere displays a variability on a wide range of space and timescales. In the tropical regions, the El-Niño–Southern Oscillation is known to play an important role at interannual timescales. In the northern extratropics, the Arctic Oscillation (AO) was found to play an important role in shaping the climate at seasonal, interannual, and decadal timescales [*Thompson and Wallace*, 1998]. The regional counterpart of the AO in the Atlantic is the North Atlantic Oscillation (NAO) that is believed to play an important role on the climatology of Europe at seasonal, interannual, and decadal timescales [*Hurrell*, 1995; *Bladé et al.*, 2011; *Smith et al.*, 2014].

Yet as discussed in *Smith et al.* [2014], the origin of this low-frequency variability is still controversial, associated either with teleconnections with the tropical Pacific variability, with the stratosphere and the quasi-biennal oscillation, with the Pacific Decadal Oscillation, with the solar 11 year cycle activity, or due to the direct interaction with the underlying Atlantic ocean surface, or a combination of these different processes.

The role of the underlying Atlantic ocean temperature dynamics has been emphasized in many investigations in the context of detailed climate models [e.g., *Mosedale et al.*, 2006; *Kravtsov et al.*, 2007; *Gastineau et al.*, 2012; *Menary et al.*, 2015], in the analysis of observations [e.g., *Czaja and Frankignoul*, 2002], and in more theoretical studies [e.g., *Gallego and Cessi*, 2000; *Marshall et al.*, 2001; *D'Andrea et al.*, 2005; *Vannitsem et al.*, 2015]. In particular, it is well established that the upper layer of the ocean, known as the mixed layer, is the place where most of the exchanges occur between the ocean and the atmosphere, namely, heat and freshwater fluxes, radiative fluxes, and momentum fluxes through wind stresses [*Wunsch and Ferrari*, 2004]. It is characterized by an almost vertically uniform profile of salinity, temperature, and density induced by a strong vertical mixing associated with the vertical instability of the water column. This instability originates not only from the heat and water fluxes but also from the wind friction and wave breaking at the ocean surface. The interaction between the atmosphere and the mixed layer is at the origin of important dynamics within the ocean [*Wunsch and Ferrari*, 2004; *Vallis*, 2006].

The properties of the ocean mixed layer (OML) are strongly seasonally dependent. In summer at midlatitudes its thickness is very small due to the weaknesses of the wind friction and the considerable heat entering at the surface, stabilizing the water column. In winter, wind friction amplifies and part of the heat is progressively lost, destabilizing the water column and inducing an increase of vertical mixing and, hence, deepening the OML. The strong seasonality is amply demonstrated in the climatologies that were developed for the mixed layer depth [*Monterey and Levitus*, 1997; *de Boyer Montégut et al.*, 2004].

The current work is an attempt to clarify the impact of the presence of the OML and of its strong seasonality on the emergence of the LFV (typically the NAO) from a dynamical system's perspective, based on the development of an appropriate low-order model and the investigation of its dynamics.

Recently, several coupled ocean-atmosphere models have been developed allowing for addressing this important problem of coupling between the upper surface of the ocean and the atmosphere [*Lorenz*, 1984; *Roebber*, 1995; *Van Veen*, 2003; *Vannitsem*, 2014a, 2014b; *Vannitsem and De Cruz*, 2014; *Vannitsem et al.*, 2015]. In the latter, a 36-variable low-order nonlinear coupled ocean-atmosphere model has been developed and shown to display a low-frequency variability (LFV) compatible with the one found for the NAO. This remarkable result points toward the important role of the Atlantic Ocean in the development of the NAO. However, the robustness of this conjecture still needs to be confirmed through the extensive investigation of this type of reduced order models, of detailed climate models, and of real data sets.

In the present paper, we discuss the impact of the seasonal variations of the radiative input of the Sun on the development of the LFV in a slightly modified version of the ocean-atmosphere model discussed in *Vannitsem et al.* [2015] in which the ocean layer is supposed to represent the OML. Besides the robustness of the LFV in the reduced order model, the analysis reveals new very important features of the nonautonomous dynamics of the model, suggesting the central role of the depth of the summer OML as the source of LFV for *all* seasons at midlatitudes and that the annual mean depth of the OML also controls the period of the LFV.

The model is briefly presented in section 2 and in the supporting information. The values of the parameters fixed in the present study are discussed in sections 2.1 and 2.2. The main results are then presented in section 3, and the potential implications of these findings for the real coupled ocean-atmosphere system are discussed in section 4.

2. The Model

The atmospheric model is based on the vorticity equations of a two-layer, quasi-geostrophic flow defined on a β plane, supplemented with a thermodynamic equation for the temperature at the interface between the two atmospheric layers. The ocean model is based on the reduced-gravity, quasi-geostrophic shallow-water model with the same order of approximation of the Coriolis parameter. The oceanic temperature is considered as a passive scalar transported by the ocean currents, but it displays strong interactions with the atmospheric temperature through radiative and heat exchanges. Since the OML is the central place of exchanges with the atmosphere, we will suppose that this shallow water ocean layer of the model only describes the mixed layer. The equations of the model are detailed in the supporting information (Text S1) and in *Vannitsem et al.* [2015].

In order to build a low-order model version, a truncated Fourier expansion approach is adopted, with a truncation at a minimal number of modes that are believed to capture key features of the observed large-scale dynamics of both the ocean and the atmosphere. Both linear and nonlinear terms in the equations of motion are then projected onto the phase subspace spanned by the modes selected, by using an appropriate scalar product (see supporting information Text S2).

The truncation leads to 20 ordinary differential equations for the atmospheric variables, 8 equations for the ocean transport dynamics, 6 equations for the temperature anomaly within the ocean, and 2 equations for the spatially averaged temperatures in the atmosphere and the ocean.

2.1. Parameter Estimation and Seasonal Variations

In the equations described in the supporting information, a large number of parameters are present whose values should be fixed in such a way to obtain realistic coupled dynamics behavior. These parameters are listed in Table 1. In order to reduce their number, let us relate some of these parameters to more fundamental parameters using the Ekman layer theory [*Houghton*, 1986; *Vallis*, 2006].

One important process is the friction at the interface between the ocean and the atmosphere. Assuming that the wind stress follows the linear relation, $(\tau_x, \tau_y) = C(u-U, v-V)$, where $(u = -\partial\psi_a^3/\partial y, v = \partial\psi_a^3/\partial x)$ are the horizontal components of the geostrophic wind and (U, V) the corresponding components of the geostrophic currents in the ocean, the wind stress curl forcing on the ocean is

$$\frac{\mathrm{curl}_z \tau}{\rho_o H} = \frac{C}{\rho_o H}\nabla^2(\psi_a^3 - \psi_o) \tag{1}$$

Table 1. Dimensional Parameters Present in the Coupled Ocean-Atmosphere Models[a]

Dynamic Atmosphere	Dynamic Ocean	Geometry	Coupling
$k_d = gC/\Delta p$ s^{-1}	$L_R = (g'H)^{1/2}/f_0$ m	$L_y = \pi L = 5000$ km	$\epsilon_a = 0.7$
$k'_d = k_d$	$r = 10^{-7}$ s^{-1}	$n = (2L_y)/L_x = 1.5$	$\lambda = c_{p,a}C$ W m^{-2} K^{-1}
$\sigma = 2.16\,10^{-6}$ J kg^{-1} Pa^{-2}	$\gamma_o = c_{p,o}\rho_o H$ J m^{-2} K^{-1}	$f_0 = 0.0001032$ s^{-1}	$d = C/(\rho_o H)$ s^{-1}
$\gamma_a = 10^7$ J m^{-2} K^{-1}		$\beta = 1.62\,10^{-11}$ m^{-1} s^{-1}	
		$\Delta p = 500$ hPa	

[a] $c_{p,a}$ and σ_B are the usual specific heat at constant pressure of the air and the Stefan-Boltzmann constant, fixed to 1004 J kg^{-1} K^{-1} and $5.6\,10^{-8}$ W m^{-2} K^{-4}, respectively. The density, ρ_o, and the specific heat at constant pressure, $c_{p,o}$, for the ocean layer are fixed to 1000 kg m^{-3} and 4000 J kg^{-1} K^{-1}. g and g' are the gravity and reduced gravity fixed to 10 and 0.031 m s^{-2}, respectively.

where $C=\rho_a C_D|\vec{v}-\vec{V}|$ with C_D is the drag coefficient, $|\vec{v}-\vec{V}|$ the norm of the relative velocity at the surface, and ρ_a the air density at the surface. The coefficient $d = C/(\rho_o H)$ characterizes the strength of the mechanical coupling between the ocean and the atmosphere, where H is the depth of the OML and ρ_o the constant density within this layer.

Similarly, one can use the Ekman layer theory to relate the coefficient k_d in equation (1) in supporting information Text S1 to the friction coefficient C in pressure coordinates as

$$k_d = \frac{gC}{\Delta p}\ \mathrm{s}^{-1} \tag{2}$$

and one assumes that $k'_d=k_d$ as in *Charney and Straus* [1980].

The heat flux parameter λ in equation (3) in supporting information Text S1 can also be related to the surface friction coefficient as discussed in *Houghton* [1986],

$$\lambda = c_{p,a}C\ \mathrm{W\,m^{-2}K^{-1}} \tag{3}$$

where $c_{p,a}$ is the specific heat at constant pressure of the air.

Let us now focus on the dependence of the different parameters of the equations within the ocean as a function of the depth of the OML, H. The first coefficient is the reduced Rossby radius of deformation, L_R, given as

$$L_R^2 = \frac{g'H}{f_0^2}\ \mathrm{m}^2 \tag{4}$$

where the reduced gravity is $g' = g(\rho_{o,2} - \rho_{o,1})/\rho_{o,1}$ and $\rho_{o,2}$ and $\rho_{o,1}$ are the densities of the deep quiet layer and the OML, respectively. It is fixed here to 0.031 m s^{-2} as in *Jiang et al.* [1995]. A second parameter that depends on H is the heat capacity,

$$\gamma_o = 4\,10^6\,H\ \mathrm{J\ m^{-2}K^{-1}} \tag{5}$$

Finally, as already mentioned above, d is inversely proportional to H. Note that γ_a depends on the depth of the atmospheric layer supposed to be fixed. Its value is chosen as in *Barsugli and Battisti* [1998], $\gamma_a = 10^7$ J m^{-2} K^{-1}.

The ensemble of parameters $\{k_d, k'_d, d, \gamma_o, \lambda, L_R\}$ can therefore be reduced to the estimation of two parameters, the depth of the ocean layer, H, and the friction coefficient, C. The latter is also assumed to be independent of the season.

2.2. Parameters of the Nonautonomous System

The radiative input at midlatitudes is clearly seasonal dependent, i.e., the system is nonautonomous. The daily dependence can be directly estimated from the astronomical parameters and the specific latitude on the Earth [e.g., *Goosse*, 2015]. The daily averaged radiative forcing for an obliquity of 23° for the domain specified in Table 1 and centered at a latitude of 45° north is displayed in Figure 1a.

As well known, the interesting features of this temporal evolution are that the amplitude of the gradient of the radiative input as a function of latitude is much smaller in summer than in winter and that latitudinal average

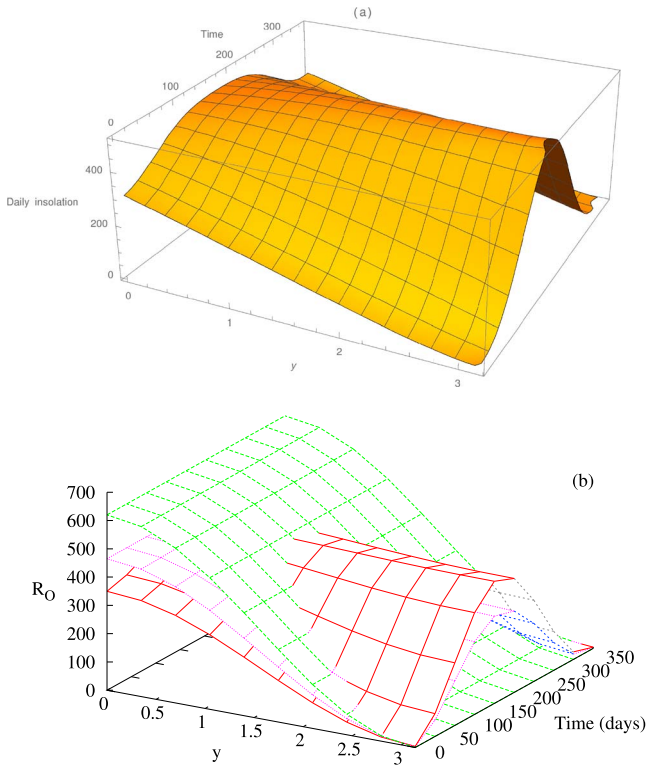

Figure 1. (a) Daily averaged insolation as obtained from *Goosse* [2015] for an obliquity of 23° and for a domain centered at a latitude of 45° with $n = 1.5$ and $\pi L = 5000$ km, as a function of latitude and time; (b) analytical expression (6) of the radiative input as a function of latitude and time for $S_o = 310\,\mathrm{W\ m^{-2}}$ and different values of κ: $\kappa = 1$ (green), $\kappa = 0.5$ (magenta), and $\kappa = 0.3$ (red). The latitude is displayed in adimensional units on the domain $[0, \pi]$. The unit along the vertical axis is W m^{-2}.

of the radiative input is smaller in winter than in summer. In order to parameterize this evolution in our model, a simple relation of the following form is used:

$$R_o = R_{o,0} + \delta R_o = S_o(1 + \alpha \sin(\omega(t - \zeta))) + \kappa S_o \cos(y)(1 - 2\alpha sin(\omega(t - \zeta))) \tag{6}$$

where $\omega = 2\pi/365$ days^{-1}, $\zeta = 80$ days, and y is the latitude in nondimensional units varying from $[0, \pi]$. κ is a free parameter and α is fixed such that the radiative input is never negative in the whole domain, $\alpha = \min((\kappa - 1)/(\kappa + 2), 0.5)$. This choice also implies that the energy input in the nonautonomous case is reaching the value of 0 at $y = \pi$ and at $t \approx 355$ days (winter solstice). Two free parameters are present in this relation: S_o, the energy input, and κ, the latitudinal contribution.

Figure 1b displays R_o for different values of κ, the smaller the value of κ, the larger the seasonal variations. For κ=0.3, the seasonal variation is very similar to the actual evolution displayed in Figure 1a. Note that for κ=1, no seasonal variability is present and corresponds to the autonomous case investigated later.

The second important parameter of the OML is H. This layer displays a strong seasonality, with a small depth in summer and a large depth in winter [e.g., *de Boyer Montégut et al.*, 2004]. *Kraus and Turner* [1967] suggested that the characteristic thickness of the convective development within the ocean is of the order of

$$H = \mu \ln(1 + \frac{B}{S}) \tag{7}$$

where B is the surface heat exchange and S is the radiative flux penetrating in the ocean layer. If the heat fluxes are time dependent, the depth H of convection is also strongly dependent on time. In the present work, we use a relation for the OML depth displaying a similar structure which allows for variations typical to the ones found in reality when a strong seasonality is present in the model,

$$H(t) = H_{\mathrm{ref}} \ln(1 + \left(\frac{500}{R_{o,0}(t)}\right)^3) \tag{8}$$

where H_{ref} is fixed to 100 m in most of the integrations performed below, unless it is explicitly stated.

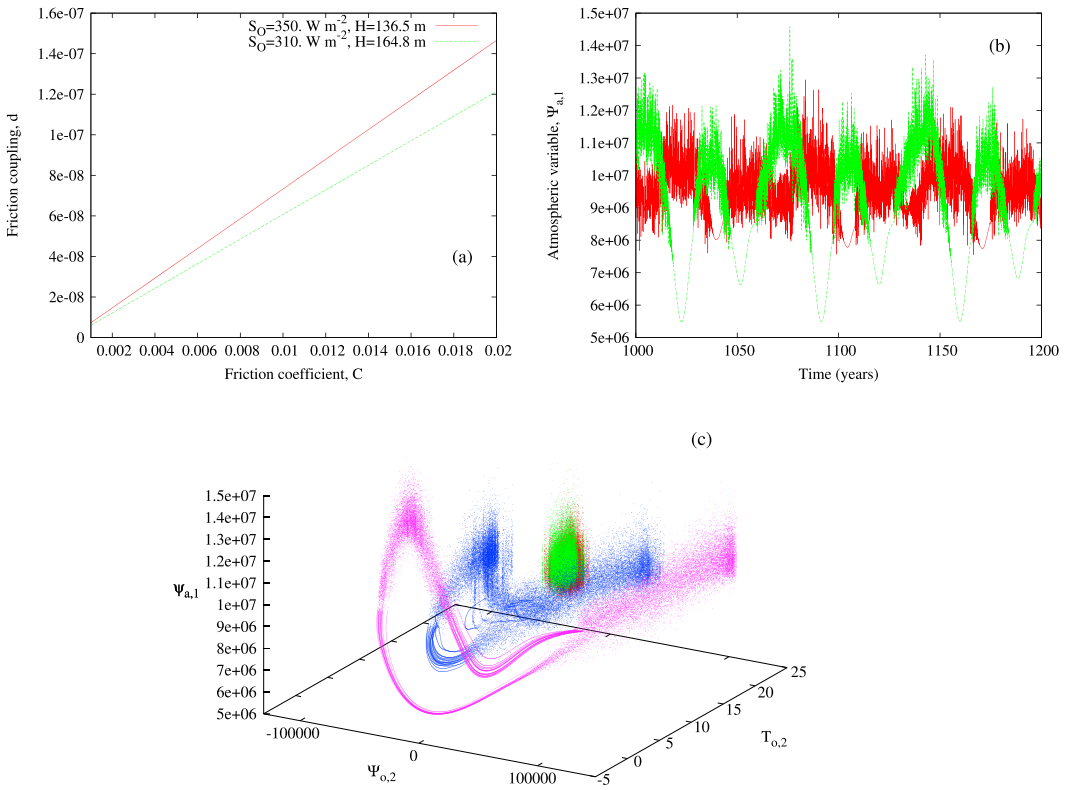

Figure 2. (a) Values of $d = C/\rho_o H$ as a function of the friction coefficient C for H =136.5 m (corresponding to S_o = 350 W m^{-2}) and 164.8 m (corresponding to S_o = 310 W m^{-2}). (b) Temporal evolution of the atmospheric barotropic streamfunction $\psi_{a,1}$ for S_o = 310 W m^{-2}, for κ = 1 and C = 0.012 (red) and 0.015 (green) kg m^{-2} s^{-1}. (c) Three-dimensional projection of the attractor in the subspace ($\psi_{o,2}, T_{o,2}, \psi_{a,1}$) for κ=1, S_o=310 W m^{-2} and different values of C, 0.01 (red), 0.011 (green), 0.012 (blue), and 0.015 (magenta) kg m^{-2} s^{-1}. The variables, ($\psi_{o,2}, T_{o,2}, \psi_{a,1}$), mainly characterize the double-gyre transport within the ocean, the meridional temperature gradient in the ocean, and the vertically averaged zonal flow within the atmosphere, respectively.

3. Results

3.1. Autonomous Version of the Model

A first integration of the model with a value of α=0., i.e., $\kappa = 1$, is performed in order to evaluate the nature of the dynamics in the absence of seasonal cycle (green surface in Figure 1b). Figure 2a displays, for reference, the values of the friction parameter $d = C/\rho_o H$ as a function of the friction coefficient C for ρ_o = 1000 kg m^{-3} and H given by equation (8) for S_o =310 and 350 W m^{-2}.

Figure 2b shows the temporal evolution after a transient period of 1000'years of the first mode, $\psi_{a,1}$, of the atmospheric barotropic streamfunction field (see supporting information Text S1) characterizing the dominant contribution of the zonal flow in the domain, for C = 0.012 and 0.015 kg m^{-2} s^{-1}. For both values of C a clear LFV signal is visible, modulating the chaotic dynamics characterizing the "weather"-scale variability. The LFV signal has a very long period of about 70 years, a value much larger than the LFV signal found in *Vannitsem et al.* [2015].

Figure 2c displays the three-dimensional (3-D) projection of several attractors for different values of C for S_o = 310 W m^{-2}. For values of C beyond 0.011 kg m^{-2} s^{-1}, a drastic change of the main location of the attractor and a drastic qualitative change of the nature of the dynamics are visible when the LFV is developing. Note that several concommittent attractors can be reached for values of C between 0.011 and 0.013 kg m^{-2} s^{-1}, depending on the initial state of the integration, as illustrated in Figure 3a in which the variance is displayed for different trajectories. The properties of these concommittent attractors are worth investigating further in the future.

The computation of the Lyapunov exponents for these cases reveals that several positive exponents are present, with a dominant exponent of 0.377 days^{-1} for C = 0.01 kg m^{-2} s^{-1}, and 0.127 days^{-1} for

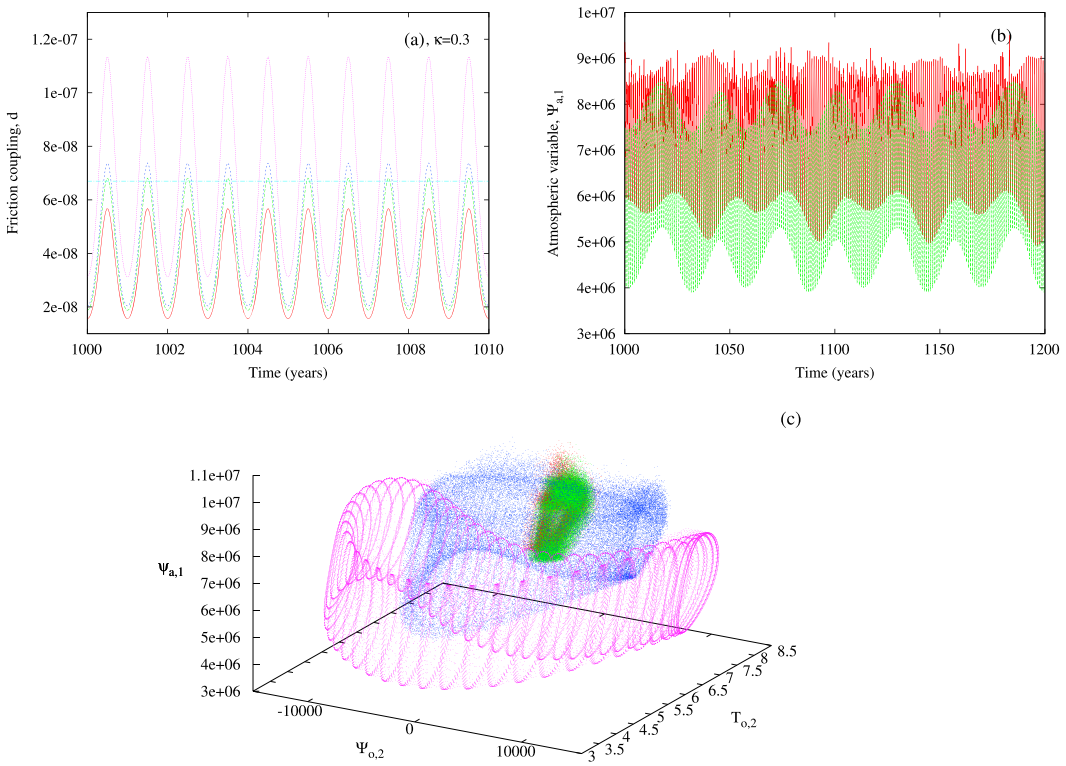

Figure 3. (a) d(t) for $\kappa = 0.3$ and for different values of C = 0.005 (red), 0.006 (green), 0.0065 (blue), and 0.010 (magenta) kg m^{-2} s^{-1}; (b) temporal evolution of the atmospheric barotropic variable, $\psi_{a,1}$, for $\kappa = 0.3$, S_o = 310 W m^{-2}, and C = 0.0065 (red) and 0.010 (green) kg m^{-2} s^{-1}; (c) Three-dimensional projection of the attractor for $\kappa = 0.3$, S_o = 310 W m^{-2}, and different values of C: 0.005 (red), 0.006 (green), 0.0065 (blue), 0.010 (magenta) kg m^{-2} s^{-1}.

$C = 0.015$ kg m^{-2} s^{-1}, indicating that the solutions are sensitive to initial state errors, i.e., display a chaotic dynamics.

The slight modifications of the dynamical equations discussed in section 2 and of the main parameter values does not modify the main conclusions of *Vannitsem et al.* [2015] concerning the development of a coupled LFV mode, except that this LFV has now a much longer period. As we will see later, the depth of the OML is effectively controlling the period of the LFV (Figure 4b).

To interpret the development of the LFV of the magenta and blue attractors of Figure 2c, let us assume that the system is starting in the region for which $\psi_{o,2}$ is close to 0 and $T_{o,2}$ close to 10 K. In this situation, the dynamics of the ocean is characterized by a system of four gyres; i.e., the variable $\psi_{o,4}$ is dominating. Subsequently, the meridional temperature gradient within the ocean (essentially given by the value $T_{o,2}$) is building up and the intensity (with positive values) of the "double-gyre" stream function variable, $\psi_{o,2}$, increases. As the meridional temperature gradient in the ocean becomes larger, the solution enters in the highly erratic zone on the right "wing" of the attractor. In this zone, important heat exchanges between the ocean and the atmosphere are occurring in order to compensate for the temperature gradient within the ocean. This in turn induces a large meridional gradient of temperature within the atmosphere, driving an intense baroclinic instability around an intense westerly jet (also leading to large local instability properties of the flow). Due to the rapid transport of heat within the atmosphere the temperature gradient within the ocean is progressively attenuated, leading to a decrease of $T_{o,2}$. The decrease of the temperature gradient within the ocean is also accompanied by a decrease of the intensity of the double-gyre variable, $\psi_{o,2}$, and a system of four gyres (with opposite sign) is again developing within the ocean. This evolution is then repeated on the left wing of the attractor. Interestingly, the growth and decay of the double gyre, with high amplitudes of $\psi_{o,2}$ in Figure 2c, and the concommittent development of the four-gyre system, is associated with the westward propagation of basin-scale Rossby-like waves.

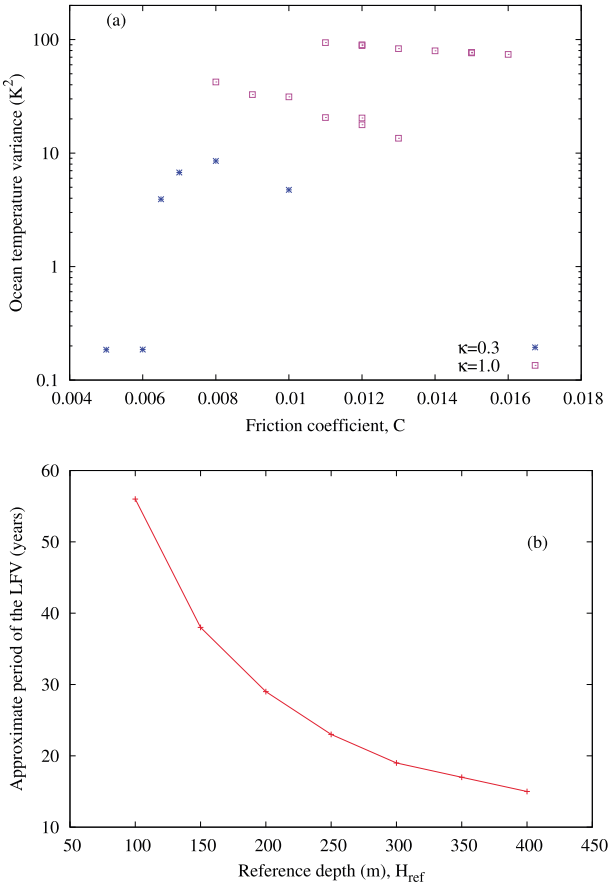

Figure 4. (a) Variance of the ocean temperature as a function of the friction coefficient, C, for the autonomous, $\kappa = 1$, and the nonautonomous, $\kappa = 0.3$, systems, complementing the phase subspace representations already displayed in Figures 2c and 3c; (b) variations of the approximate period of the LFV as a function of H_{ref} for the nonautonomous case, $\kappa = 0.3$, with $S_o = 310$ W m^{-2}.

To summarize, the dynamics seems therefore the consequence of the interplay between the transport of heat within the ocean, the heat fluxes between the ocean and the atmosphere, and the wind friction inducing the development of Rossby-like waves within the ocean. A detailed investigation of this specific dynamics is worth performing to clarify the roles of the different processes at play through the evaluation of the energetics of this system in the spirit of *Gallego and Cessi* [2000] and *Farneti and Vallis* [2013].

3.2. Nonautonomous Version

Let us now turn to the model version in which the seasonal signal is incorporated. For the present analysis, we fix $\kappa = 0.3$, implying that $\alpha = 0.4375$ in (6). The solar radiative input into the ocean corresponds to the red surface in Figure 1b. Figure 3a displays the evolution of the friction coefficient $\mathrm{d}(t) = C/(\rho_o H(t))$ as a function of time for different values of C. A reference value of d as obtained for κ=1., $S_o = 310$ W m^{-2}, and $C = 0.011$ kg m^{-2} s^{-1} is also displayed (see Figure 2a). In winter the friction parameter d is small and progressively amplifies in the course of the year with a maximum value in summer. As for the autonomous case, no LFV is developing for small values of C. However, once this parameter reaches a value larger than 0.065, the LFV appears as illustrated in Figures 3b and 3c, but with a smaller amplitude. Interestingly, this LFV is now developing for values of C smaller than in the autonomous case. Moreover, the qualitative change occurs when the amplitude of d reaches *in summer* a value larger than the reference value of the autonomous case for which the LFV is emerging ($d = 6.7\ 10^{-8}$ s^{-1}, horizontal line in Figure 3a). Furthermore, this LFV persists in winter even if d becomes much smaller than the reference value of the autonomous case.

This result suggests that the LFV is essentially driven by the depth of the OML in summer and that the inertia of the ocean is sufficiently important to avoid a strong response to the fast decrease of the friction parameter d in winter.

As mentioned above, the period of the LFV is large in the current parameter settings (Table 1) and differs considerably to the one obtained in *Vannitsem et al.* [2015] for which the depth of the ocean was fixed to $H = 500$ m. To understand this feature, we have modified the OML reference depth, H_{ref} in equation (8) from 100 to 400 m. The OML can now reach very large mean depth for H_{ref} large, with values similar to the one used in *Vannitsem et al.* [2015].

Figure 4b shows the approximate period of the LFV as a function of H_{ref}. The larger is H_{ref}, the shorter is the period. This result is consistent with the period obtained in *Vannitsem et al.* [2015] of about 22 years and suggests that the mean climatological depth of the OML (associated with its inertia) is controlling the period of the LFV.

To interpret this behavior, one must recall that the succession of double and quadruple gyres in the system is associated with a Rossby-like wave propagation. In the classical theory of Rossby wave propagation for finite deformation radius, L_d, the frequency of the Rossby wave ω is given by

$$\omega = \frac{-k\beta}{K^2 + 1/L_d^2} \tag{9}$$

where k is the zonal wave number and $K^2 = l^2 + k^2$, the square of the total wave number with l the meridional wave number. If we consider basin-scale modes (as it is our aim in the present system), then this frequency is approximately proportional to L_d^2, or in other words to the depth H. This feature qualitatively explains the result found here with a decrease of the period of the LFV with H_{ref} in the ocean-atmosphere model. We can therefore associate this property with the propagation of basin-scale Rossby-like waves within the OML.

4. Discussion

The coupled dynamics between the ocean mixed layer and the atmosphere is described using a reduced order coupled nonlinear ocean-atmosphere model with seasonal variations of the radiative input. The coupled low-frequency variability mode discovered in *Vannitsem et al.* [2015] is a robust feature for both the autonomous and nonautonomous versions of this reduced order ocean-atmosphere model, suggesting further the genuine character of the LFV in the coupled ocean-atmosphere system. Remarkably, the period of this LFV is much longer than the one discovered in *Vannitsem et al.* [2015] and, as shown here, is closely related to the reference depth of the OML, the deeper is the layer, the shorter is the period and the smaller the amplitude of the LFV. This feature can be interpreted in terms of Rossby-like wave propagation.

An even more important finding is that in the nonautonomous version of the model, the LFV is controlled by the depth of the OML in the summer period during which the layer thickness is small. Furthermore, once the LFV is settled, it does not disappear in the course of the year when the layer thickness is much larger. To interpret this result, one must realize that the ocean has an important inertia and that the LFV has a period much larger than the one of the annual cycle. This large difference in frequencies seems to preclude the possibility of complex interactions between the two dominant modes of variability present in the model dynamics. The possibility of synchronizations to the annual cycle is however worth investigating in the context of this model in the future.

The finding that the LFV is controlled by the properties of the interaction between the ocean and the atmosphere during the summer period is intriguing and is worth exploring further. Usually, in data analysis, the focus is given to the dynamics in winter because the LFV signal-to-noise ratio is larger, except in a limited number of investigations [e.g., *Bladé et al.*, 2011]. An analysis of the data during the full seasonal cycle is worth performing in the light of the present results.

In the real coupled ocean-atmosphere system, the mean depth and the amplitude of the seasonal variations of the OML strongly depend on the location in the Atlantic (and more generally at midlatitudes in the Northern Hemisphere). We can therefore wonder whether depending on the location in the North Atlantic, the amplitude and frequency of the LFV could change, provided that the different zones are sufficiently decoupled; or if a dominant global LFV is selected for the whole North Atlantic zone. This question is worth addressing in the future in both observational data and in the current model in which spatial dependences of the mixed layer depth can be introduced.

Acknowledgments
This work has benefited from enlightening discussions with Michael Ghil and Valerio Lucarini. The low-order model is available upon request (Stephane.Vannitsem@meteo.be). This work is partially supported by the Belgian Federal Science Policy Office under contract BR/12/A2/STOCHCLIM.

References

Barsugli, J. J., and D. S. Battisti (1998), The basic effects of atmosphere-ocean thermal coupling on midlatitude variability, *J. Atmos. Sci.*, *55*, 477–493.

Bladé, I., B. Liebmann, D. Fortuny, and G.-J. van Oldenborgh (2011), Observed and simulated impacts of the summer NAO in Europe: Implications for projected drying in the Mediterranean region, *Clim. Dyn.*, *39*, 709–727, doi:10.1007/s00382-011-1195-x.

Charney, J. G., and D. M. Straus (1980), Form-drag instability, multiple equilibria and propagating planetary waves in baroclinic, orographically forced, planetary wave systems, *J. Atmos. Sci.*, *37*, 1157–1176.

Czaja, A., and C. Frankignoul (2002), Observed impact of Atlantic SST anomalies on the North Atlantic Oscillations, *J. Clim.*, *15*, 606–623.

D'Andrea, F., A. Czaja, and J. Marshall (2005), Impact of anomalous ocean heat transport on the North Atlantic Oscillation, *J. Clim.*, *18*, 4955–4969.

de Boyer Montégut, C., G. Madec, A. Fisher, A. Lazar, and D. Iudicone (2004), Mixed layer depth over the global ocean: An examination of profile data and a profile-based climatology, *J. Geophys. Res.*, *109*, C12003, doi:10.1029/2004JC002378.

Farneti, R., and G. Vallis (2013), Meridional energy transport in the coupled Atmosphere-Ocean system: Compensation and partitioning, *J. Clim.*, *26*, 7151–7166.

Gallego, B., and P. Cessi (2000), Exchanges of heat and momentum between the atmosphere and the ocean: A minimal model of decadal oscillations, *Clim. Dyn.*, *16*, 479–489.

Gastineau, G., F. D'Andrea, and C. Frankignoul (2012), Atmospheric response to the North Atlantic Ocean variability on seasonal to decadal time scales, *Clim. Dyn.*, *40*, 2311–2330, doi:10.1007/s00382-012-1333-0.

Goosse, H. (2015), *Climate System Dynamics and Modelling*, Cambridge Univ. Press, New York.

Houghton, J. T. (1986), *The Physics of the Atmospheres*, Cambridge Univ. Press, Cambridge, U. K.

Hurrell, J. (1995), Decadal trends in the North Atlantic Oscillation: Regional temperatures and precipitation, *Science*, *269*(5224), 676–679, doi:10.1126/science.269.5224.676.

Jiang, S., F.-F. Jin, and M. Ghil (1995), Multiple equilibria, periodic, and aperiodic solutions in a wind-driven, double-gyre, shallow-water model, *J. Phys. Oceanogr.*, *25*, 764–786.

Kraus, E. B., and J. S. Turner (1967), A one-dimensional model of the seasonal thermocline: II. The general theory and its consequences, *Tellus*, *19*, 98–106.

Kravtsov, S., W. K. Dewar, P. Berloff, M. Ghil, and J. C. McWilliams (2007), A highly nonlinear coupled mode of decadal variability in a mid-latitude ocean-atmosphere model, *Dyn. Atmos. Oceans*, *43*, 123–150, doi:10.1016/j.dynatmoce.2006.08.01.

Lorenz, E. N. (1984), Formulation of a low-order model of a moist general circulation, *J. Atmos. Sci.*, *41*, 1933–1945.

Marshall, J., H. Johnson, and J. Goodman (2001), A study of the interaction of the North Atlantic Oscillation with ocean circulation, *J. Clim.*, *14*, 1399–1421.

Menary, M., D. Hodson, J. Robson, R. Sutton, and R. Wood (2015), A mechanism of internal decadal Atlantic Ocean variability in a high-resolution coupled climate model, *J. Clim.*, *28*, 7764–7785, doi:10.1175/JCLI-D-15-0106.1.

Monterey, G., and S. Levitus (1997), *Seasonal Variability of Mixed Layer Depth for the World Ocean*, 100 pp., NOAA Atlas NESDIS 14, Natl. Oceanic and Atmos. Admin., Silver Spring, Md.

Mosedale, T., D. Stephenson, M. Collins, and T. Mills (2006), Granger causality of coupled climate processes: Ocean feedback on the North Atlantic Oscillation, *J. Clim.*, *19*, 1182–1194.

Roebber, P. J. (1995), Climate variability in a low-order coupled atmosphere-ocean model, *Tellus A*, *47*, 473–494.

Smith, D. M., A. A. Scaife, R. Eade, and J. R. Knight (2014), Seasonal to decadal prediction of the winter North Atlantic Oscillation: Emerging capability and future prospects, *Q. J. R. Meteorol. Soc.*, doi:10.1002/qj.2479.

Thompson, D. W. J., and J. M. Wallace (1998), The Arctic Oscillation signature in the wintertime geopotential height and temperature fields, *Geophys. Res. Lett.*, *25*, 1297–1300.

Vallis, G. (2006), *Amospheric and Oceanic Fluid Dynamics*, Cambridge Univ. Press, Cambridge, U. K.

Vannitsem, S. (2014a), Dynamics and predictability of a low-order wind-driven ocean-atmosphere coupled model, *Clim. Dyn.*, *42*, 1981–1998, doi:10.1007/s00382-013-1815-8.

Vannitsem, S. (2014b), Stochastic modelling and predictability: Analysis of a low-order coupled ocean-atmosphere model, *Philos. Trans. R. Soc., A, 372*, 20130282, doi:10.1098/rsta.2013.0282.

Vannitsem, S., and L. De Cruz (2014), A 24-variable low-order coupled ocean-atmosphere model: OA-QG-WS v2, *Geosci. Model Dev.*, *7*, 649–662, doi:10.5194/gmd-7-649-2014.

Vannitsem, S., J. Demaeyer, L. de Cruz, and M. Ghil (2015), Low-frequency variability and heat transport in a low-order nonlinear coupled ocean-atmosphere model, *Physica D*, *309*, 71–85, doi:10.1016/j.physd.2015.07.006.

Van Veen, L. (2003), Overturning and wind driven circulation in a low-order ocean-atmosphere model, *Dyn. Atmos. Oceans*, *37*, 197–221.

Wunsch, C., and R. Ferrari (2004), Vertical mixing, energy, and the general circulation of the ocean, *Annu. Rev. Fluid Mech.*, *36*, 281–314.